ORIGINAL ARTICLE

ANATOMICAL SOCIETY   Journal of Anatomy   WILEY

Disruption of tight junctions contributes to hyposalivation of salivary glands in a mouse model of type 2 diabetes

Yan Huang[1] | Qian-Ying Mao[1] | Xi-Jin Shi[2] | Xin Cong[2] | Yan Zhang[2] |
Li-Ling Wu[2] | Guang-Yan Yu[1] | Ruo-Lan Xiang[2]

[1]Department of Oral and Maxillofacial Surgery, Peking University School and Hospital of Stomatology, National Engineering Laboratory for Digital and Material Technology of Stomatology, Beijing, China

[2]Department of Physiology and Pathophysiology, Peking University School of Basic Medical Sciences, Key Laboratory of Molecular Cardiovascular Sciences, Ministry of Education, and Beijing Key Laboratory of Cardiovascular Receptors Research, Beijing, China

Correspondence
Guang-Yan Yu, National Engineering Laboratory for Digital and Material Technology of Stomatology, Department of Oral and Maxillofacial Surgery, Peking University School and Hospital of Stomatology, Beijing 100081, China.
Email: gyyu@263.net

Ruo-Lan Xiang, Key Laboratory of Molecular Cardiovascular Sciences, Ministry of Education, and Beijing Key Laboratory of Cardiovascular Receptors Research, Department of Physiology and Pathophysiology, Peking University School of Basic Medical Sciences, Beijing 100191, China.
Email: xiangrl@bjmu.edu.cn

Funding information
National Natural Science Foundation of China, Grant/Award Number: 81570993, 81671005 and 81974151

Abstract

Tight junction (TJ) plays an important role in regulating paracellular fluid transport in salivary glands; however, little is known about the involvement of TJs in diabetes salivary glands. This study aimed to investigate the alterations of TJs and their possible contribution in diabetes-induced hyposalivation. Here, we observed that the morphologies of submandibular glands (SMGs) were impaired, characterized by enlarged acini accumulation with giant secretory granules, which were significantly reduced in atrophic ducts in SMGs of db/db mice, a spontaneous model of type-2 diabetes. However, the secretory granules were increased and scattered in the acini of diabetes parotid glands (PGs). Other ultrastructural damages including swollen mitochondria, expansive endoplasmic reticulum, and autophagosomes were observed in the diabetes group. The levels of TJ proteins including claudin-1 (Cldn1) and claudin-3 (Cldn3) were increased, whereas those of claudin-4 (Cldn4), occludin (Ocln), and zonula occludens-1 (ZO-1) were decreased in SMGs of db/db mice. Higher Cldn1 and Cldn3 and lower claudin-10 (Cldn10) and Ocln levels were observed in PGs of diabetes mice. Taken together, the structures of SMGs and PGs were impaired in diabetes mice, and the disruption of TJ integrity in both SMGs and PGs may contribute to diabetes-induced hyposalivation.

KEYWORDS

diabetes, saliva, salivary gland, submandibular gland, tight junction

1 | INTRODUCTION

Saliva plays a critical role in the maintenance of oral and systemic health through its diverse functions such as providing lubrication, initiating digestion, and offering first-line immunity (Dawes et al., 2015). Diabetes is one of the most prevalent metabolic diseases affecting millions of people (Cho et al., 2018). Dry mouth is a common complication of diabetes (Hoseini et al., 2017; Carramolino-Cuellar et al., 2018; Pedersen et al., 2018). Studies show that the prevalence rate of dry mouth is up to 30%–80% in diabetes patients and only 10%–30% in healthy subjects (Carda et al., 2006; Ivanovski et al., 2012; Malicka et al., 2014). Moreover, components of saliva have been reported to be altered in diabetes patients, which may change oral microenvironment and make it susceptible to bacteria (Naseri et al., 2018; Salehi et al., 2019; Tiongco et al., 2019). Reduced salivary flow can cause damage to the oral cavity and induce diseases like dental caries, oral infections, swallowing difficulties, and speaking difficulties, which in turn affect the quality of patient life (Dawes et al., 2015, Marsh et al., 2016,

Mauri-Obradors *et al.*, 2017). Ameliorating hyposalivation can therefore largely improve life quality of patients with diabetes. However, the mechanism of diabetes-induced hyposalivation is not yet fully understood; hence, it is of great significance to investigate the underlying mechanisms of diabetes hyposalivation.

Saliva is mainly secreted from three major salivary glands namely the submandibular glands (SMGs), parotid glands (PGs), and sublingual glands (SLGs) through a tight junction (TJ)-based paracellular pathway and an aquaporin 5 (AQP5)-mediated transcellular pathway (Liu and Lin, 1969). Recently, reduced expression of AQP5 has been reported in diabetes patients and animal models (Zhang *et al.*, 2013; Huang *et al.*, 2018); however, little is known about the changes in the paracellular pathway in diabetes salivary glands. TJs are the protein complex located at the cell-to-cell interactions, which consist by transmembrane proteins, such as claudins (Cldns) and occludin (Ocln), together with intracellular proteins, like zonula occludens (ZOs) (Zhang *et al.*, 2018). TJs mediate water, ions and small molecules passing through the paracellular pathway, and play an important role in salivary secretion (Zhang *et al.*, 2013; Xiang *et al.*, 2014; Cong *et al.*, 2015; Buckley and Turner, 2018). In hyposecretory SMG, acinar TJ width is decreased, while the expression of ZO-1, Cldn3, and Cldn11 are reduced (Cong *et al.*, 2012; Yang *et al.*, 2017). Additionally, both epithelial and endothelial TJs are disrupted in salivary glands of patients with Sjögren's syndrome (SS) as well as model mice, contributing to salivary hyposecretion (Zhang *et al.*, 2016; Cong *et al.*, 2018). Moreover, TJs are reportedly damaged in other diabetes complications (Jiang *et al.*, 2019; Bu *et al.*, 2020). Cldn1 is upregulated in streptozotocin-induced mice podocytes, which contributes to the pathogenesis of albuminuria (Hasegawa *et al.*, 2013). Down-regulation of TJ proteins Cldn5, Ocln, and ZO-1 are observed in vascular endothelial cells of cerebral tissue in KKAy mice, a genetic model of type-2 diabetes (Li *et al.*, 2018). Even in the early stage of type-2 diabetes, TJ structures are reported to be impaired in distal intestinal epithelia (Beltrame de Oliveira *et al.*, 2019). These findings imply that the abnormality of TJ is an important mechanism related to the pathogenesis of diabetes complications. However, whether TJs are altered in diabetes salivary glands and involved in diabetes-induced hyposalivation or not is still unknown.

Based on this background, this study aimed to investigate the morphological alterations of the three major salivary glands in type-2 diabetes mice and the role of TJs in diabetes-induced hyposalivation, providing novel insights into diabetes-induced hyposalivation and availing a potential target for ameliorating dry mouth in diabetes patients.

2 | MATERIALS AND METHODS

2.1 | Reagents and antibodies

Alcian Blue 8GX, Schiff's reagent and Oil red O staining solution were purchased from Sigma-Aldrich. The primary antibodies to Cldn1 (BS1063), Cldn3 (BS1067), Cldn4 (BS1068) and claudin-7 (Cldn7, BS1070) were purchased from Bioworld Technology (Minneapolis, MN, USA). Primary antibodies to Cldn10 (38-8400), Ocln (71-1500), ZO-1 (40-2200) and Alexa-Fluor-594-conjugated secondary antibodies were from Thermo Fisher Scientific. The antibody to β-actin (#4970) was purchased from Cell Signaling Technology (Beverly, MA, USA).

2.2 | Animals

Six 16-week-old male leptin receptor knock-out db/db mice and six age-matched db/m mice were provided by ChangZhou Cavens Laboratory Animal Ltd. The animal research was approved by the Ethics Committee of Animal Research, Peking University Health Science Center (No. LA2015071) and complied with the ARRIVE guidelines (Group, 2010) as well as the relevant national laws on the protection of animals. Mice were kept in a humidity-and temperature (24 ℃)-controlled animal room with a light-dark cycle (12:12 hr) in different cages for each group (3/cage). The animals were allowed free access to normal diet (complete formula feed, 12.95% fat, 24.02% protein and 63.03% carbohydrate, purchased from BEIJING KEAO XIELI FEED CO., LTD.) and drinking water ad libitum but were fasted for a minimum of 5 hr with water ad libitum before extraction. After anesthesia with an intraperitoneal injection of chloral hydrate (0.4 g/kg body weight), the volume of saliva was measured for 10 min after injection of pilocarpine (10 μg/g body weight) using capillary tubes. Total protein content of collected saliva was detected using the BCA Protein Assay Kit (M&C Gene Technology). SMGs, PGs and SLGs were isolated and extracted from db/m and db/db mice at 9:00–12:00 a.m. Blood glucose level was measured on mice tail veins using a Glucometer (ACCU-CHEK). Blood samples were collected from the heart and the serum was isolated by centrifuging at 2,975 *g* for 10 min at 4°C. The level of serum insulin was measured with the Iodine [125I]-Insulin Radioimmunoassay Kit (Union Medical & Pharmaceutical Technology Ltd.). Assessment of insulin resistance index (HOMA-IR) was calculated according to the following formula: fasting insulin (mU/L) × fasting glucose (mmol/L)/22.5. Finally, mice were sacrificed by spinal dislocation.

2.3 | Histological evaluation

SMG, PG and SLG tissues from mice were fixed in 4% paraformaldehyde for 24 hr, embedded in paraffin wax, and cut into serial sections of 5 μm. The sections were deparaffinized and hydrated, then stained with hematoxylin and eosin (H&E). To determine the components of the secretory granules, the deparaffinized and hydrated series sections were immersed in 1% alcian blue (AB) (pH 2.5) for 15 min. After rinsing in water, the sections were counterstained with hematoxylin. For periodic acid-Schiff (PAS) staining, deparaffinized and hydrated sections were oxidized in 1% periodic acid solution for 10 min and rinsed in distilled water, after which the sections were placed in Schiff reagent for 15 min and their nucleus were counterstained. Fresh SMG, PG and SLG samples were embedded in optimal cutting temperature compound and cut into frozen slices of 7 μm by

a cryostat for Oil red O staining. Images of the glands were captured under a light microscope (Q550CW, Leica, Manheim, Germany). Five fields of each section were randomly chosen to evaluate the size of acini and ducts in mice SMGs. The mean size of each section was statistically analyzed.

2.4 | Transmission electron microscopy

Animal tissues of salivary glands were fixed in 2% glutaraldehyde at 4°C for 24 hr and post-fixed in 1% osmium tetroxide at 4°C for 2 hr. Ultrathin sections were produced and stained with 10% uranyl acetate and 1% lead citrate. The ultrastructure was observed under a transmission electron microscope (TEM) (HITACHI H-7000, Tokyo, Japan). Ten acinar cells and ten ductal cells of each sample were randomly selected to analyze the size and number of secretory granules in mice SMGs and PGs.

2.5 | Western blotting

The samples were homogenized in RIPA buffer (Thermo Fisher Scientific) and sonicated for 27 s (run 3 s and pause 2 s), then centrifuged at 17,136 g for 10 min at 4°C. The supernatant was collected, and the protein concentration was determined by the Bradford method (M&C Gene Technology Ltd). Equal amounts of proteins (20-40 µg) were separated on a 10% and 12% SDS-PAGE at a stable voltage 100 V for about 2 hr and transferred onto a polyvinylidene difluoride membrane at a stable electric current of 200 mA for 2-3 hr. The membranes were blocked with 5% non-fat milk for 2 hr at room temperature, probed with the primary antibodies at 4°C overnight, and incubated with horseradish peroxidase (HRP)-conjugated secondary antibodies for 2 hr at room temperature. Immunoreactive bands were visualized with enhanced chemiluminescence (Thermo Scientific Pierce), and their densities were quantified using Image J Software (National Institutes of Health).

2.6 | Reverse transcription PCR and real-time PCR

Total RNA was extracted from homogenized gland tissue using TRIzol reagent (Invitrogen). For each sample, 1-2 µg RNA was reversed into cDNA by 5 × All-In-One RT MasterMix (G490, Applied Biological Materials Inc) according to the manufacturer's instructions. For real-time PCR, 2 × SYBR® Green Master Mix (Genstar) was used with 10 nmol/L of each primer, and 2 µl of each 1:3 diluted cDNA, in a final volume of 10 µl. DyNAmo™ ColorFlash SYBR Green qPCR Kit (Thermo Fisher Scientific) was used on a PikoReal Real-Time PCR System (Thermo Fisher Scientific) cycling at 95°C × 5 min, 95°C × 10 s, followed by 60°C × 30 s for 40 cycles, after which analysis was done using PikoReal 2.0 software. The primer sequences for TJ components were as shown in Table 1.

2.7 | Immunofluorescence staining

Gland samples were fixed in 4% paraformaldehyde for 24 hr at 4°C, dehydrated in 30% sucrose and embedded in optimal cutting temperature compound. Frozen slices of 7 µm were cut in a cryostat and immersed in citrate buffer (pH 6.0) then heated in a microwave oven for 15 min for antigen retrieval. After blockage with 1% bovine serum albumin, the sections were incubated by the primary antibodies with dilution 1:100 or 1:200 in 1% bovine serum albumin at 4°C overnight. Secondary antibodies with dilution 1:400 in phosphate-buffered saline were incubated at 37°C for 1 hr. Nuclei were stained with 4′,6-diamidino-2-phenylindole (DAPI). Confocal images were captured by using a laser scanning confocal microscope (Leica TCS SP8, Wetzlar, Germany).

2.8 | Statistical analysis

Data are described as mean ± standard error of the mean. The normality of data in db/m and db/db mice was confirmed by Shapiro-Wilk test. Statistical significance of the difference between db/m

TABLE 1 Primers for tight junction proteins

Gene	Forward primer (5′-3′)	Reverse primer (5′-3′)
Mouse		
Cldn1	GACAGGAGCAGGAAAGTAGGA	CTTTGGAATTAGGCAGAACGA
Cldn2	CCATGGCCTCCCTTGGCGTCC	CACACATACCCAGTCAGGCTG
Cldn3	TTTCTTTGTCCATTCGGCTTG	ACCGTACCGTCACCACTACCA
Cldn4	GATCTTGGCCTTGACGGTCTC	CTCTGGATGAACTGCGTGGTG
Cldn5	CCATGGGGTCTGCAGCGTTGG	GGCGAACCAGCAGAGCGGCAC
Cldn7	CCATGGCCAACTCGGGCCTGCAAC	TCACACGTATTCCTTGGAGG
Cldn10	CCATGGGTAGCACGGCCTTGG	TTAGACATAGGCATTTTTATC
Ocln	CCATCTTTCTTCGGGTTTTCA	CTTCTGGATCTATGTACGGCTCA
ZO-1	GTAAAGCCTGGTGGTGGAACT	TCGAACCTCTACTCTACGACATG
β-actin	CACAGCTGAGAGGGAAATC	TCAGCAATGCCTGGGTAC

Abbreviations: Cldn, claudin; Ocln, occuldin; ZO-1, zonula occludens-1.

and db/db mice was evaluated using unpaired Student's *t* test with GraphPad software (GraphPad Prism 5.0, CA, USA). All *p* < .05 were considered to be significant.

3 | RESULTS

3.1 | Impaired morphology and function of salivary glands in db/db mice

The clinical and biochemical parameters of mice are presented in Table 2. The body weight was increased in db/db mice in which increased food and water intake, higher blood glucose, serum insulin, and HOMA-IR value confirmed diabetes (Table 2). Despite the higher body weight and larger size of db/db mice (Figure 1a), gross observation showed that the size of both SMGs and PGs

were obviously decreased in db/db mice (Figure 1b). The average weight of SMGs was 92.08 ± 5.75 mg in db/m mice, whereas a lower weight of 45.50 ± 7.18 mg was observed in db/db mice (Figure 1c). Meanwhile, the weight of PGs was significantly reduced from 15.50 ± 1.18 mg in db/m mice to 6.68 ± 0.75 mg in db/db mice (Figure 1d). However, no changes were observed in SLGs of db/db mice (12.67 ± 1.86 mg) as compared with db/m mice (13.58 ± 2.71 mg) (Figure 1e). In addition, the ratios of gland weight to body weight were decreased in SMGs, PGs and SLGs (Figure 1f–h). Therefore, a significant atrophy of salivary glands was presented in db/db mice.

In order to evaluate the function of salivary glands in diabetic condition, we measured the stimulated salivary flow rates of mice after injection of pilocarpine. As shown in Figure 1i, the stimulated salivary flow rates were significantly decreased in db/db mice compared to db/m mice (Figure 1i). Moreover, the total salivary protein

TABLE 2 The clinical and biochemical parameters of mice

Group	Body weight (g)	Water intake (ml/day)	Food intake (g/day)	Blood glucose (mmol/L)	Serum insulin (mU/L)	HOMA-IR
db/m	34.73 ± 1.20	7.50 ± 0.79	3.44 ± 0.09	7.80 ± 0.68	12.76 ± 1.87	4.15 ± 0.71
db/db	56.12 ± 3.07**	13.13 ± 0.63**	4.84 ± 0.24**	24.47 ± 1.37**	21.63 ± 1.58**	24.33 ± 1.33**

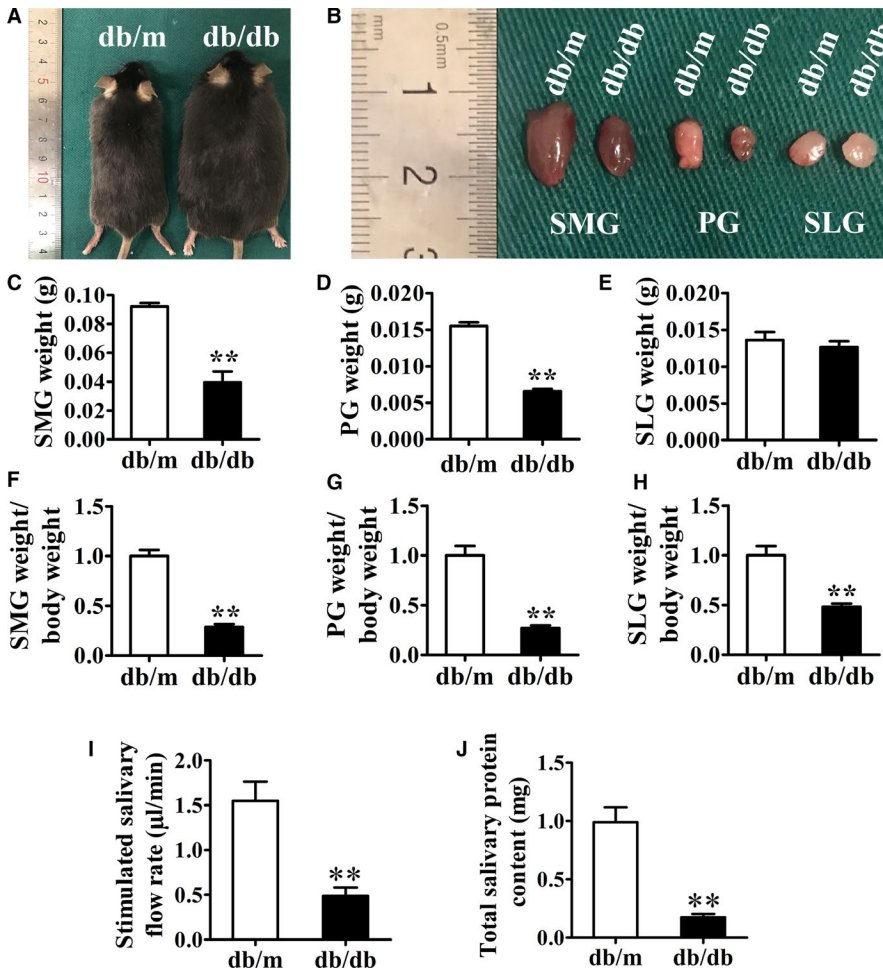*Note:* Mean ± *SEM*, *n* = 5–6, **p* < .01, versus db/m.

FIGURE 1 Gross morphology and function of submandibular glands, parotid glands and sublingual glands in db/m and db/db mice. (a) Picture of mice. (b) Picture of the three major salivary glands from mice. (c–e) Weight of the glands of SMGs, PGs and SLGs. (f–h) The ratio of gland weight to body weight of SMGs, PGs and SLGs. (i) Stimulated salivary flow rates of db/m and db/db mice. (j) Total salivary protein content from db/m and db/db mice. PG, parotid gland; SLG, sublingual gland; SMG, submandibular gland. Data are presented as mean ± *SEM*; *n* = 4–6, **p* < .01 compared with db/m mice

content in collected saliva was also reduced in db/db mice (Figure 1j). Taken together, the secretory function of diabetes salivary glands was impaired.

3.2 | Impaired structure of submandibular glands and parotid glands in db/db mice

We investigated the histological features of the three major salivary glands. H&E staining showed an enlargement of acini and an atrophy of ducts in SMGs of db/db mice (Figure 2a). The mean size of acini was 73.35 ± 2.45 μm² in db/m mice, which increased to 139.10 ± 5.54 μm² in db/db mice while the ductal size reduced from 260.90 ± 9.25 μm² in db/m mice to 204.0 ± 6.174 μm² in db/db mice (Figure S1). No alterations were observed in the size of acini

and ducts of diabetes PGs and SLGs (Figure 2b,c). Oil red O staining showed no accumulation of lipid droplets in SMGs, PGs and SLGs (Figure 2d–f). The acidic and neutral mucin can be detected by AB and PAS staining, respectively (Filipe and Branfoot, 1974). As shown in Figure 2g,j, acini of SMGs were moderately stained by AB and PAS reagents in db/m mice but strong staining was observed in db/db mice, indicating that more acidic and neutral mucins accumulated in the acini of diabetes SMGs (Figure 2g,j). The AB staining for PG acini in both db/m and db/db mice was negative. However, PAS staining intensity was slightly stronger in the acini of db/db mice compared to db/m group, indicating that more neutral mucins were blocked in the acini of diabetes PGs (Figure 2h,k). As shown in Figure 2i,l, the acini of mice SLGs had strongly positive AB and PAS staining results in db/m group, suggesting that SLGs acini contain much more acidic and neutral mucins than SMGs and PGs. However, no
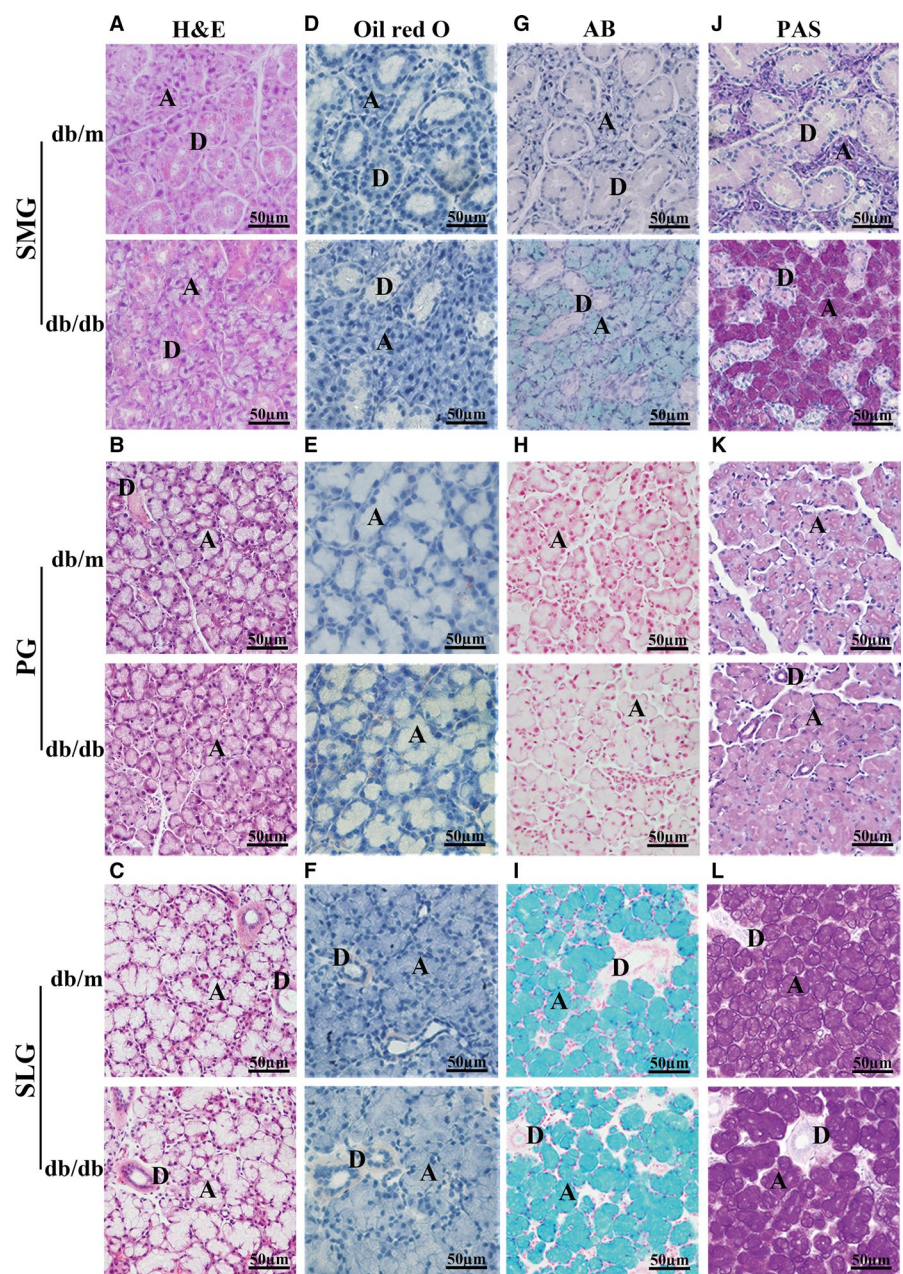

FIGURE 2 Histological structure of submandibular glands, parotid glands and sublingual glands in db/m and db/db mice. (a–c) H&E staining of SMGs, PGs and SLGs. (d–f) Oil red O staining of SMGs, PGs and SLGs. (g–i) Alcian blue (AB) staining of SMGs, PGs and SLGs. (j–l) Periodic acid-Schiff (PAS) staining of SMGs, PGs and SLGs. A, acinus; D, duct; PG, parotid gland; SLG, sublingual gland; SMG, submandibular gland
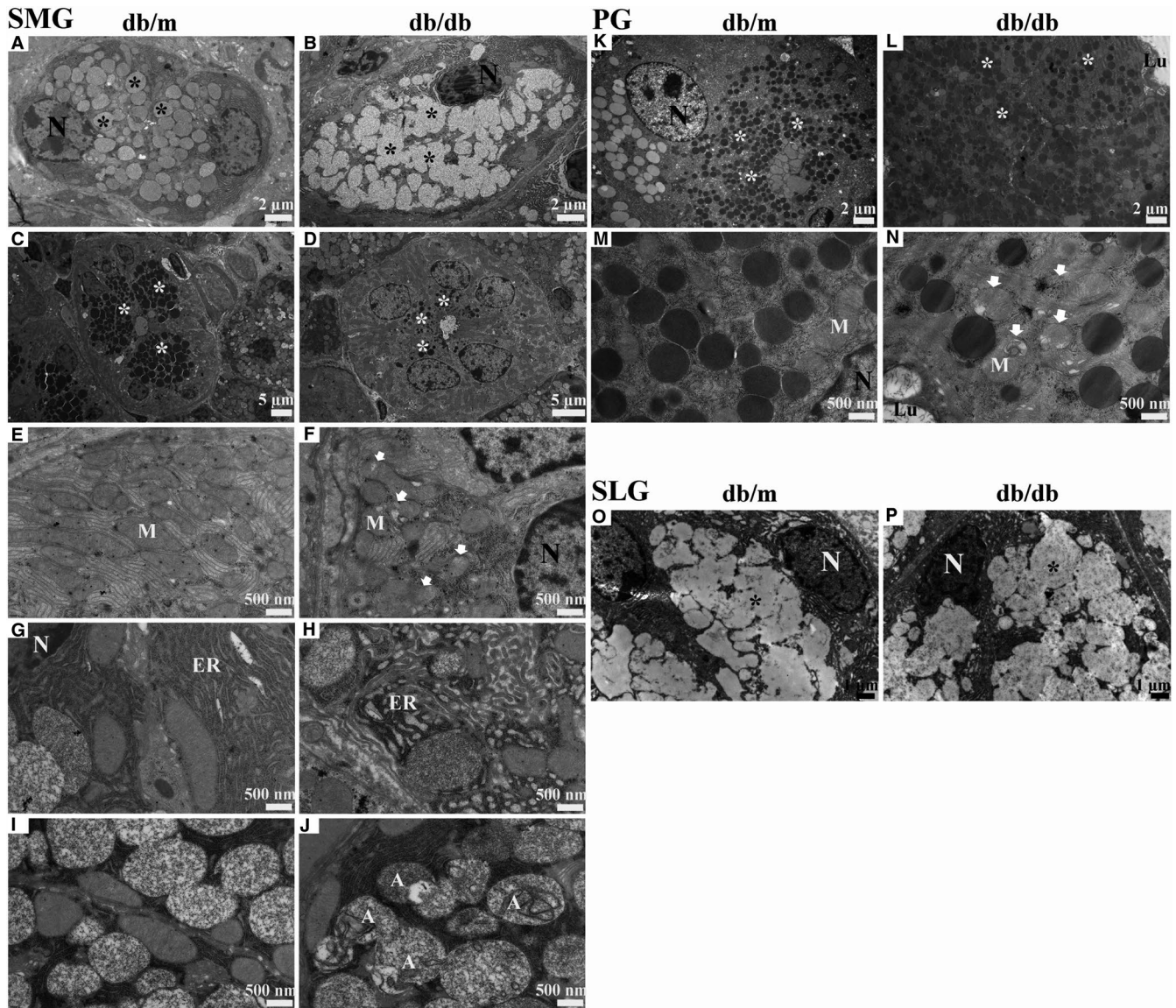
FIGURE 3 Ultrastructure of submandibular glands, parotid glands and sublingual glands in db/m and db/db mice. (a, b) Acini of SMGs in db/m and db/db mice. (c, d) Granular convoluted tubules (GCTs) of SMGs in db/m and db/db mice. (e, f) Mitochondria in SMGs of db/m and db/db mice. (g, h) Endoplasmic reticulum in SMGs of db/m and db/db mice. (i, j) Autophagosomes in SMGs of db/m and db/db mice. (k, l) Acini of PGs in db/m and db/db mice. (m, n) Mitochondria in PGs of db/m and db/db mice. (o, p) Acini of SLGs in db/m and db/db mice. A, autophagosomes; ER, endoplasmic reticulum; Lu, lumen; M, mitochondria; N, nucleus; PG, parotid gland; SLG, sublingual gland; SMG, submandibular gland; *, secretory granules; white arrows represent swollen and raptured mitochondria

obvious differences were observed between db/m and db/db group (Figure 2i,l).

3.3 | Injured ultrastructure of submandibular glands and parotid glands in db/db mice

TEM showed that round and homogenous secretory granules with a mean diameter of 1.11 ± 0.05 μm occupied in the acinar cells of SMGs in db/m mice (Figure 3a, Figure S2). However, secretory granules with lower densities fused to each other, and formed relatively large pools of secretory material (diameter around 3.20 ± 0.25 μm) in the acinar cells of db/db mice (Figure 3b, Figure S2). Moreover, normal endoplasmic reticulum appearance was displayed in the cytoplasm of db/m mice, while irregular dilation around the nuclei of acinar cells was observed in the SMGs of db/db mice (Figure 3a,b). The granular convoluted tubule (GCT) is a major component of the ductal system in mouse SMG. Here, the number of secretory granules in GCTs was significantly decreased in the SMGs of db/db mice (25 ± 2.22/ cell in db/db mice against 45.00 ± 1.39/cell in db/m mice, $p < .01$) (Figure 3c,d, Figure S3). Swollen and ruptured mitochondria (white arrows), as well as expansive rough endoplasmic reticulum, were also observed in the SMGs of db/db mice (Figure 3e–h). Additionally, more autophagosomes were detected in the acini of db/db mice compared to db/m mice (Figure 3i,j). Similar to SMGs, the ultrastructural characters of PGs presented more secretory granules and impaired

FIGURE 4 Expression of tight junction proteins in submandibular glands of db/m and db/db mice. (a) The mRNA expression of Cldn1, Cldn2, Cldn3, Cldn4, Cldn5, Cldn7, Cldn10, Ocln, and ZO-1 in SMGs of db/m and db/db mice. (b) The protein levels of Cldn1, Cldn3, Cldn4, Cldn7, Cldn10, Ocln, and ZO-1 in SMGs of db/m and db/db mice. (c–h) Immunofluorescence staining of Cldn1 (c), Cldn3 (d), Cldn4 (e), Cldn7 (f), Ocln (g), and ZO-1 (h) in SMGs of db/m and db/db mice. Cldn, claudin; Ocln, occludin; SMG, submandibular gland; ZO-1, zonula occludens-1. Data are presented as mean ± *SEM*; n = 6, *p < .05; **p < .01 compared with db/m mice
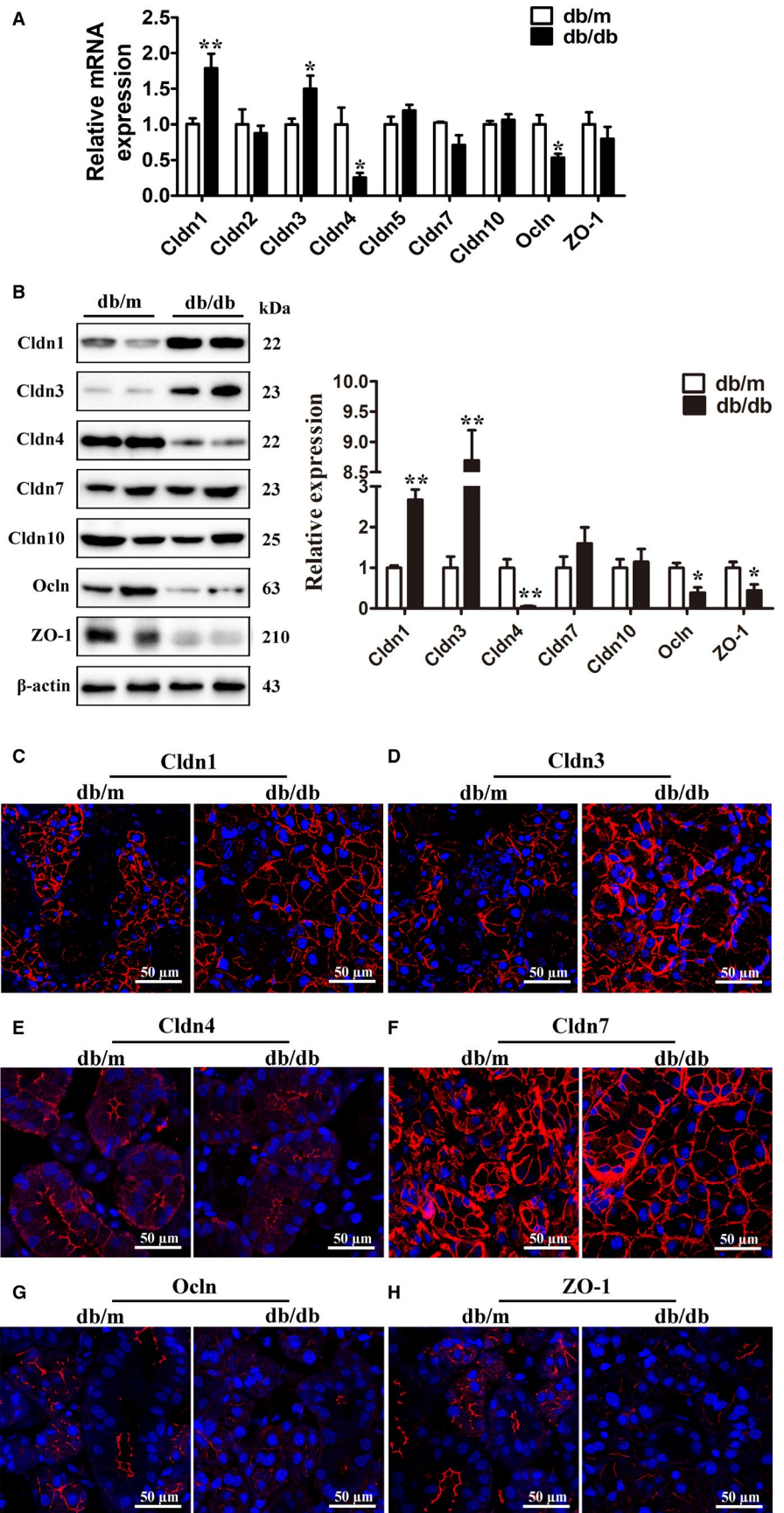
mitochondria in the acini of db/db mice. The number of secretory granules was 96 ± 3.89/cell in acinar cells of db/m mice PG, while db/db mice had 109 ± 3.32/cell (Figure S4). In line with PAS staining, the secretory granules in the acini of PGs were concentrated in the apical area of db/m mice, which were more dispersed in the acini of db/db mice (Figure 3k–n). No obvious differences were observed in the ultrastructure of SLGs between db/m and db/db mice (Figure 3o,p).

3.4 | The changes in tight junction protein expression in submandibular glands of db/db mice

Cognizant of the importance of TJs in salivary secretion, we evaluated the expression and distribution of TJ proteins in SMGs. The levels of Cldn1 and Cldn3 mRNA were enhanced, whereas Cldn4 and Ocln mRNA levels were reduced in the SMGs of db/db mice while no significant changes were detected in Cldn2, Cldn5, Cldn7, Cldn10, and ZO-1 mRNA levels (Figure 4a). Similarly, the protein levels of Cldn1 and Cldn3 were much higher in db/db mice than in db/m mice, whereas the expression of Cldn4, Ocln, and ZO-1 were lower in the SMGs of db/db mice. The amounts of Cldn7 and Cldn10 were not changed (Figure 4b).

Furthermore, we analyzed the distributions of TJ proteins. Immunofluorescence images showed that Cldn1, Cldn3 and Cldn7 were mainly located in apicolateral and basolateral plasma membrane of both acini and ducts. Cldn4 was predominantly expressed in the apicolateral membrane of ducts in mouse SMG (Figure 4c–f). Ocln and ZO-1 were predominantly expressed in the apicolateral area in both

acinar and ductal cells (Figure 4g,h). The fluorescence intensities of Cldn1 and Cldn3 were enhanced in the db/db group (Figure 4c,d) but Cldn4 staining intensity was reduced in the ducts of diabetes SMGs (Figure 4e). Moreover, the staining intensities of Ocln and ZO-1 were much weaker in the acini of diabetes SMGs (Figure 4g,h). Apart from changes in TJ protein expression, changes in their subcellular locations also affect salivary secretion. However, no obvious alterations were observed in the locations of TJ proteins in diabetes SMGs in this study.

3.5 | The changes in tight junction protein expression in parotid glands of db/db mice

The expression levels of TJ proteins in PGs were further examined. Cldn10 and Ocln mRNA levels were decreased in the PGs of db/db mice (Figure 5a). Consistent with mRNA alterations, the protein expression of Cldn10 and Ocln were largely reduced, and Cldn1 and Cldn3 protein levels were elevated in diabetes PGs. Other TJ proteins including Cldn2, Cldn4, Cldn5, Cldn7, and ZO-1 were unchanged in the PGs of db/db mice when compared to db/m mice (Figure 5b).

4 | DISCUSSION

In this study, we analyzed the morphological alterations of the three major salivary glands in diabetes mice. Our results suggested
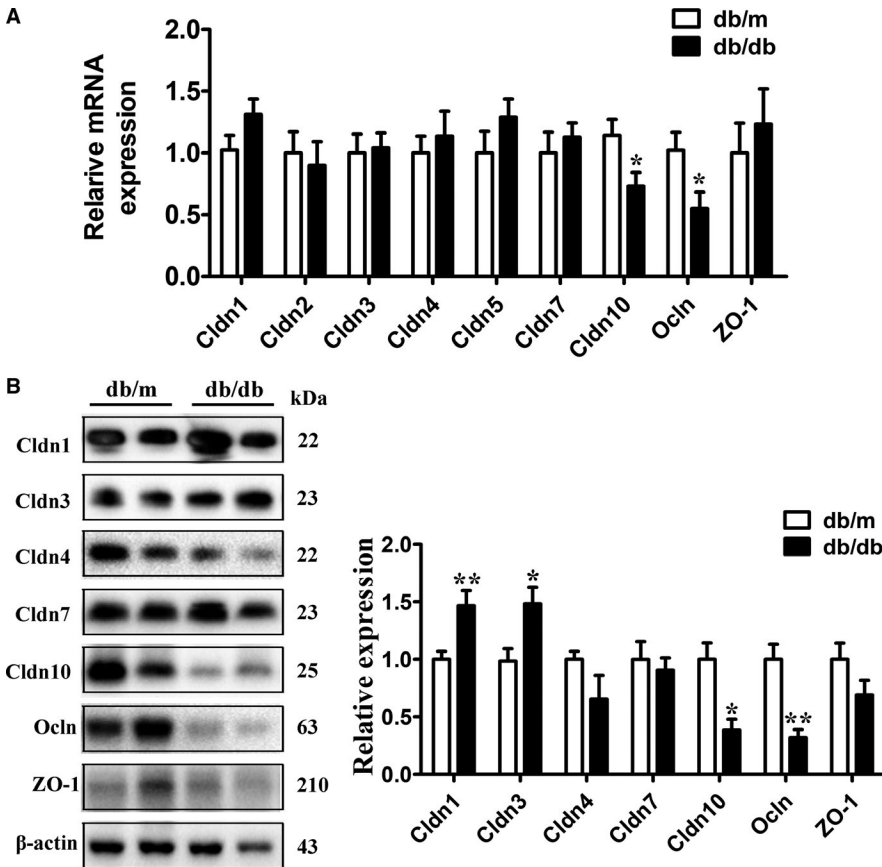

FIGURE 5 Expression of tight junction proteins in parotid glands of db/m and db/db mice. (a) The mRNA expression of Cldn1, Cldn2, Cldn3, Cldn4, Cldn5, Cldn7, Cldn10, Ocln, and ZO-1 in PGs of db/m and db/db mice. (b) The protein levels of Cldn1, Cldn3, Cldn4, Cldn7, Cldn10, Ocln, and ZO-1 in PGs of db/m and db/db mice. PG, parotid gland; Cldn, claudin; Ocln, occludin; ZO-1, zonula occludens-1. Data are presented as mean ± *SEM*; *n* = 6. *$p <$ .05; **$p <$ .01 compared with db/m mice

that the structures were impaired in both diabetes SMGs and PGs. Furthermore, by detecting TJ proteins in SMGs and PGs, we found increased expression of Cldn1 and Cldn3 and decreased expression of Cldn4, Ocln, and ZO-1 in diabetes SMGs, while higher expression of Cldn1 and Cldn3 and lower levels of Cldn10 and Ocln were measured in diabetes PGs. These TJ protein changes in diabetes SMGs and PGs may lead to the disruption of TJ integrity and affect the secretory functions of salivary glands. Moreover, the different changes in TJ protein expression in diabetes SMGs and PGs indicated that the mechanisms under the dysfunction of diabetes SMGs and PGs were variable.

Previous studies have demonstrated the impairments in the structure and function of salivary glands in diabetes patients and animal models. Clinical pathological observations showed the enlargement of acini and secretory granules in SMGs from diabetes patients. In contrast, increased volume fractions of stromal components including vessels, and proportionally less parenchyma have been reported in previous studies (Lindeberg and Andersen, 1987; Reuterving et al., 1987; Lilliu et al., 2015a, 2015b). In addition, lipid droplets and secretory granules reportedly accumulate in the acinar and ductal cells in SMGs of diabetes patients (Anderson and Garrett, 1986; Anderson et al., 1994). In rats with streptozotocin-induced diabetes and insulin resistant rats induced by a high-fat diet, degenerative changes in the structure and reduced function of both SMG and PG have been observed (Kolodziej et al., 2017; Maciejczyk et al., 2017). PGs from diabetes patients are characterised by the presence of small acini, increased number of intracytoplasmic lipid droplets in the acinar and ductal cells, as well as an abundant adipose infiltration in the stroma (Anderson and Garrett, 1986; Carda et al., 2005). However, other reserchers found no changes in the size of acini and secretory granules in diabetes PGs (Lilliu et al., 2015a, 2015b). Therefore, controversy still exists in the nature of the alterations of diabetes salivary glands. The different observations among these studies may be related to the stages or types of diabetes. Here, we used type-2 diabetes model db/db mice to explore the morphological alterations of the three major salivary glands in diabetic condition. Obvious atrophy of SMGs and PGs were observed in db/db mice when compared to db/m mice. SMGs showed an atrophy of ducts in diabetes mice and an enlargment of acini caused by accumulation of mucins. Acini of murine SMGs are composed of seromucous cells, which are moderately stained by AB and PAS reagents (Filipe and Branfoot, 1974). Here, stronger AB and PAS staining densities of acini in db/db mice demonstrated that more acidic and neutral mucins accumulated in the acini of diabetes SMG. As for PGs, acini of murine PGs are mainly composed of serous cells, which display AB-negative and moderate PAS-positive (Filipe and Branfoot, 1974). In our results, although no changes in the size of acini were observed, more neutral mucins were dipersed in acinar cells of diabetes PGs. Mucins are the main component of saliva that can be altered when salivary glands are in a pathological state, therefore they can reflect changes in salivary glands functions (High et al., 1985). Therefore, accumulation of mucins in both acini of diabetes SMG and PG demonstrated that secretory functions of SMG and PG were impaired in diabetic

condition. Moreover, the stimulated salivary flow rates were notably decreased in db/db mice, further suggesting reduced secretory functions of diabetes salivary glands.

Ultrastructurally, large secretory granules were accumulated in the acini of diabetes SMGs, and more were scattered in the acini of diabetes PGs. Proteins are the main component of secretory granules and their secretion is a dynamic process comprising synthesis, transport, and secretion (Suzuki and Iwata, 2018). Here, the docked secretory granules in diabetes SMG and PG suggested that the process of secretion is somehow impaired in diabetic condition. However, no obvious alterations were detected in diabetes SLGs. Even if, in mucous cells of human labial glands, statistical analysis revealed that the reactivity for statherin was significantly lower in the samples from diabetes subjects than from subjects without diabetes (Isola et al., 2011). The different results between human and mouse mucous cell may due to species diversity. Normally, SMG contributes to more than 60% of resting salivary secretion while PG contributes only about 25% of resting saliva (Pedersen et al., 2018). However, salivary production of PG increased to about 53% under the stimulation of the parasympathetic nervous system (Cunning et al., 1998; Pathak et al., 2004, Brazen et al., 2020). Therefore, the different roles of SMG and PG in resting and stimulated conditions may account for their discordant structural changes in diabetes. Previous studies also identified an atrophy of both SMGs and PGs in alloxan-induced and streptozotocin-induced diabetes rats (High et al., 1985; Reuterving et al., 1987). Increased proportional volumes of acini and decreased proportional volumes of the granular ducts, as well as an accumulation of secretory granules are also reported in SMGs from diabetes rats (High et al., 1985; Anderson et al., 1994). The difference was that no lipid droplets were detected in our results, which may be due to the difference in animal models. Other ultrastructural alterations including ruptured mitochondria and expansive endoplasmic reticulum, as well as more autophagosomes were measured in diabetes SMGs and PGs, demonstrating that the ultrastructures of SMGs and PGs were significantly injured by diabetes.

The morphological impairments of SMGs and PGs are relevent to their functions. TJ-based paracellular fluid secretion largely represents the functions of salivary glands, which play a dynamic role in salivary secretion (Peppi and Ghabriel, 2004; Baker, 2016; Yano et al., 2017). The expression and organization of TJ proteins are altered during several pathological processes of xerostomia (Ewert et al., 2010; Mellas et al., 2015; Ding et al., 2017; Cong et al., 2018; Zhang et al., 2019). In salivary glands of SS patients and NOD mice, the integrity of TJs is disrupted, including elevated Cldn1 and Cldn3 expression as well as reduced Cldn4, Ocln, and ZO-1 expression (Zhang et al., 2016). ZO-1 is also observed to be decreased in post-irradiated human SMG (Nam et al., 2016). Moreover, the expression of ZO-1, Cldn3, and Cldn11 are reduced in the hyposecretory SMG, whereas these TJ proteins levels are reversed with the restoration of SMG function (Cong et al., 2012; Yang et al., 2017). Therefore, these findings suggest that TJ proteins are important in the process of salivary secretion, but whether TJs are altered in diabetes-induced hyposalivation or not is still unclear. The present

study found that the expression of Cldn1 and Cldn3 were increased, while Cldn4, Ocln, and ZO-1 expression were decreased in diabetes SMGs. Cldn1, Cldn3 and Cldn4 were classified to pore-sealing Cldns in Cldn family. They fucntion as a barier to stop water, ions and molecules from passing through, which would decrease permeability of the epithelium (Khan and Asif, 2015; Amoozadeh et al., 2017). Therefore, the higher expression of Cldn1 and Cldn3 might stop saliva components passing through the acinar epithelium and reduce salivary secretion in diabetes SMGs. Since Cldn4 is predominantly located in the apicolateral membrane of ductal cells in mouse SMG, decreased Cldn4 may increased water and ion resorptions from primary saliva, which further reduces saliva secretion. Studies in diabetes retinal vessels revealed that reduced Ocln and ZO-1 increased retinal endothelial permeability, which causes diabetic retinopathy (Jiang et al., 2017). Ocln and ZO-1 are also reported to be decreased in blood-brain barrier vessels under diabetic conditions, which increases the permeability of the blood-brain barrier, and increases the risk of diabetic neurological complications (Yoo et al., 2016). Therefore, decreased Ocln and ZO-1 in diabetes SMGs might also contribute to diabetes-induced hyposalivation. However, the exact roles of these alterations in diabetes hyposalivation still need further investigation.

The changes in TJs in PG have rarely been previously explored. In our study, injured morphologies of diabetes PGs suggested that the secretory function of PGs was damaged in diabetic condition. Our study revealed that Cldn1 and Cldn3 were upregulated, while Cldn10 and Ocln were downregulated in db/db mice. Cldn10 was reported to be pore-forming claudins, which can increase TJ permeability (Khan and Asif, 2015; Amoozadeh et al., 2017). Therefore, lower Cldn10 level might reduce TJ permeability and inhibit salivation through the paracellular pathway. All together, the alterations of Cldn1, Cldn3, Cldn10 and Ocln expression might contribute to the disruption of TJ, which is involved in the dysfunction of diabetes PGs.

There were several limitations in our study. Firstly, all the results are based on mouse experiments. As is known, there are differences between the structures of human and mouse salivary glands. The human SMG is a mixed gland mainly composed of serous acini while mouse SMG is composed of seromucous acini. Therefore, the results in our study may not fully reflect the changes in human body. Secondly, our results suggested that morphological changes of SMG, PG, and SLG were different under diabetic condition, however the mechanism is not clear. Other researchers found that serous acini are more vulnerable to diabetes than mucous acini (Anderson and Garrett, 1986; Kamata et al., 2007). Herein, the differently composed acini of SMG, PG and SLG may be the reasons, but this needs further investigations. In addition, the mechanisms by which diabetes alters TJ protein expression and reduces secretory granules secretion in mice SMGs and PGs also need more investigations. Our future work will focus on these three aspects for better understanding of the mechanism on diabetes-induced hyposalivation. Moreover, since mice were just fasted for 5 hr, and eating food is known to stimulate salivary secretion, the secretory function of salivary glands might be influenced by the stimulation of food.

The present study revealed that the morphologies of SMG and PG were damaged in diabetes, characterized by acinar accumulation of secretory granules. Moreover, the integrity of TJs was disrupted in both diabetes SMGs and PGs, evidenced by higher Cldn1 and Cldn3 levels, as well as lower Cldn4, Ocln, and ZO-1 levels in diabetes SMGs. Furthermore, higher Cldn1 and Cldn3 levels and lower Cldn10 and Ocln levels were observed in diabetes PGs. The injured TJs in SMG and PG might be responsible for diabetes hyposalivation. Insulin resistance is a main characteristic and major pathogenesis of type 2 diabetes and its complications, here, all the alterations observed in salivary glands might be related to severe insulin resistance in db/db mice. The results of our study provided new insights into diabetes-induced hyposalivation and revealed potential targets for helping improve life quality of diabetes patients.

AUTHOR CONTRIBUTIONS

Yan Huang contributed to the design of the work, acquisition and analysis of data as well as drafting the manuscript. Qian-Ying Mao and Xi-Jin Shi contributed to the acquisition of data and revising the manuscript. Cong Xin and Yan Zhang contributed to the interpretation of data and revising the manuscript. Li-Ling Wu, Guang-Yan Yu and Ruo-Lan Xiang contributed to the conception and design of the work, interpretation of data and revising the manuscript. All authors declare no competing interests.

DATA AVAILABILITY STATEMENT

All data generated by this study are included in the manuscript and accompanying supplementary material.

ORCID

Yan Huang https://orcid.org/0000-0002-0126-7810

REFERENCES

Amoozadeh, Y., Dan, Q., Anwer, S., Huang, H.H., Barbieri, V., Waheed, F. et al. (2017) Tumor necrosis factor-alpha increases claudin-1, 4, and 7 expression in tubular cells: role in permeability changes. Journal of Cellular Physiology, 232, 2210–2220.

Anderson, L.C. and Garrett, J.R. (1986) Lipid accumulation in the major salivary glands of streptozotocin-diabetic rats. Archives of Oral Biology, 31, 469–475.

Anderson, L.C., Suleiman, A.H. and Garrett, J.R. (1994) Morphological effects of diabetes on the granular ducts and acini of the rat submandibular gland. Microscopy Research and Technique, 27, 61–70.

Baker, O.J. (2016) Current trends in salivary gland tight junctions. Tissue Barriers, 4, e1162348.

Beltrame de Oliveira, R., Matheus, V.A., Canuto, L.P., De Sant'ana, A. and Collares-Buzato, C.B. (2019) Time-dependent alteration to the tight junction structure of distal intestinal epithelia in type 2 prediabetic mice. Life Sciences, 238, 116971.

Brazen, B., Dyer, J. (2020). *Histology, Salivary Glands*. Treasure Island, FL: StatPearls Publishing LLC.

Bu, J., Yu, J., Wu, Y., Cai, X., Li, K., Tang, L. et al. (2020) Hyperlipidemia affects tight junctions and pump function in the corneal endothelium. *American Journal of Pathology*, 3, 563–576.

Buckley, A. and Turner, J.R. (2018) Cell biology of tight junction barrier regulation and mucosal disease. *Cold Spring Harbor Perspectives in Biology*, 10, a029314.

Carda, C., Carranza, M., Arriaga, A., Díaz, A., Peydró, A. and Gomez de Ferraris, M.E. (2005) Structural differences between alcoholic and diabetic parotid sialosis. *Medicina Oral, Patología Oral y Cirugía Bucal*, 10, 309–314.

Carda, C., Mosquera-Lloreda, N., Salom, L., Gomez de Ferraris, M.E. and Peydró, A. (2006) Structural and functional salivary disorders in type 2 diabetic patients. *Medicina Oral, Patología Oral y Cirugía Bucal*, 11, E309–314.

Carramolino-Cuellar, E., Lauritano, D., Silvestre, F.J., Carinci, F., Lucchese, A. and Silvestre-Rangil, J. (2018) Salivary flow and xerostomia in patients with type 2 diabetes. *Journal of Oral Pathology and Medicine*, 47, 526–530.

Cho, N.H., Shaw, J.E., Karuranga, S., Huang, Y., da Rocha Fernandes, J.D., Ohlrogge, A.W. et al. (2018) IDF diabetes atlas: global estimates of diabetes prevalence for 2017 and projections for 2045. *Diabetes Research and Clinical Practice*, 138, 271–281.

Cong, X., Zhang, X.M., Zhang, Y., Wei, T., He, Q.-H., Zhang, L.-W. et al. (2018) Disruption of endothelial barrier function is linked with hyposecretion and lymphocytic infiltration in salivary glands of Sjögren's syndrome. *Biochimica et Biophysica Acta (BBA) - Molecular Basis of Disease*, 1864, 3154–3163.

Cong, X., Zhang, Y., Li, J., Mei, M., Ding, C., Xiang, R.-l. et al. (2015) Claudin-4 is required for modulation of paracellular permeability by muscarinic acetylcholine receptor in epithelial cells. *Journal of Cell Science*, 128, 2271–2286.

Cong, X., Zhang, Y., Shi, L., Yang, N.-Y., Ding, C., Li, J. et al. (2012) Activation of transient receptor potential vanilloid subtype 1 increases expression and permeability of tight junction in normal and hyposecretory submandibular gland. *Laboratory Investigation*, 92, 753–768.

Cunning, D.M., Lipke, N. and Wax, M.K. (1998) Significance of unilateral submandibular gland excision on salivary flow in noncancer patients. *Laryngoscope*, 108, 812–815.

Dawes, C., Pedersen, A.M., Villa, A., Ekström, J., Proctor, G.B., Vissink, A. et al. (2015) The functions of human saliva: a review sponsored by the World Workshop on Oral Medicine VI. *Archives of Oral Biology*, 60, 863–874.

Ding, C., Cong, X., Zhang, X.M., Li, S.-L., Wu, L.-L. and Yu, G.-Y. (2017) Decreased interaction between ZO-1 and occludin is involved in alteration of tight junctions in transplanted epiphora submandibular glands. *Journal of Molecular Histology*, 48, 225–234.

Ewert, P., Aguilera, S., Alliende, C., Kwon, Y.-J., Albornoz, A., Molina, C. et al. (2010) Disruption of tight junction structure in salivary glands from Sjögren's syndrome patients is linked to proinflammatory cytokine exposure. *Arthritis and Rheumatism*, 62, 1280–1289.

Filipe, M.I. and Branfoot, A.C. (1974) Abnormal patterns of mucus secretion in apparently normal mucosa of large intestine with carcinoma. *Cancer*, 34, 282–290.

Hasegawa, K., Wakino, S., Simic, P., Sakamaki, Y., Minakuchi, H., Fujimura, K. et al. (2013) Renal tubular sirt1 attenuates diabetic albuminuria by epigenetically suppressing claudin-1 overexpression in podocytes. *Nature Medicine*, 19, 1496–1504.

High, A.S., Sutton, J. and Hopper, A.H. (1985) A morphometric study of submandibular salivary gland changes in streptozotocin-induced diabetic rats. *Archives of Oral Biology*, 30, 667–671.

Hoseini, A., Mirzapour, A., Bijani, A. and Shirzad, A. (2017) Salivary flow rate and xerostomia in patients with type I and II diabetes mellitus. *Electron Physician*, 9, 5244–5249.

Huang, Y., Shi, X., Mao, Q., Zhang, Y., Cong, X., Zhang, X. et al. (2018) Aquaporin 5 is degraded by autophagy in diabetic submandibular gland. *Science China Life Sciences*, 61, 1049–1059.

Isola, M., Lantini, M., Solinas, P., Diana, M., Isola, R., Loy, F.et al. (2011) Diabetes affects statherin expression in human labial glands. *Oral Diseases*, 17, 685–689.

Ivanovski, K., Naumovski, V., Kostadinova, M., Pesevska, S., Drijanska, K. and Filipce, V. (2012) Xerostomia and salivary levels of glucose and urea in patients with diabetes. *Prilozi*, 33, 219–229.

Jiang, Q.W., Kaili, D., Freeman, J., Lei, C.-Y., Geng, B.-C., Tan, T. et al. (2019) Diabetes inhibits corneal epithelial cell migration and tight junction formation in mice and human via increasing ROS and impairing Akt signaling. *Acta Pharmacologica Sinica*, 40, 1205–1211.

Jiang, Y., Liu, L. and Steinle, J.J. (2017) Compound 49b regulates ZO-1 and occludin levels in human retinal endothelial cells and in mouse retinal vasculature. *Investigative Ophthalmology & Visual Science*, 58, 185–189.

Kamata, M., Shirakawa, M., Kikuchi, K., Matsuoka, T. and Aiyama, S. (2007) Histological analysis of the sublingual gland in rats with streptozotocin-induced diabetes. *Okajimas Folia Anatomica Japonica*, 84, 71–76.

Khan, N. and Asif, A.R. (2015) Transcriptional regulators of claudins in epithelial tight junctions. *Mediators of Inflammation*, 2015, 219843.

Kolodziej, U., Maciejczyk, M., Miasko, A., Matczuk, J., Knaś, M., Żukowski, P. et al. (2017) Oxidative modification in the salivary glands of high fat-diet induced insulin resistant rats. *Frontiers in Physiology*, 8, 20.

Li, Y., Li, Q., Pan, C.S., Yan, L., Hu, B.-H., Liu, Y.-Y. et al. (2018) Bushen huoxue attenuates diabetes-induced cognitive impairment by improvement of cerebral microcirculation: involvement of RhoA/ROCK/moesin and Src signaling pathways. *Frontiers in Physiology*, 9, 527.

Lilliu, M.A., Loy, F., Cossu, M., Solinas, P., Isola, R. and Isola, M. (2015a) Morphometric study of diabetes related alterations in human parotid gland and comparison with submandibular gland. *Anatomical Record (Hoboken)*, 298, 1911–1918.

Lilliu, M.A., Solinas, P., Cossu, M., Puxeddu, R., Loy, F., Isola, R. et al. (2015b) Diabetes causes morphological changes in human submandibular gland: a morphometric study. *Journal of Oral Pathology and Medicine*, 44, 291–295.

Lindeberg, H. and Andersen, L. (1987) The size and composition of the submandibular glands in late-onset diabetes. *Arch Otorhinolaryngol*, 244, 100–103.

Liu, F.T. and Lin, H.S. (1969) Role of insulin in body growth and the growth of salivary and endocrine glands in rats. *Journal of Dental Research*, 48, 559–567.

Maciejczyk, M., Kossakowska, A., Szulimowska, J., Klimiuk, A., Knaś, M., Car, H. et al. (2017) Lysosomal exoglycosidase profile and secretory function in the salivary glands of rats with streptozotocin-induced diabetes. *Journal of Diabetes Research*, 2017, 9850398.

Malicka, B., Kaczmarek, U. and Skoskiewicz-Malinowska, K. (2014) Prevalence of xerostomia and the salivary flow rate in diabetic patients. *Advances in Clinical and Experimental Medicine*, 23, 225–233.

Marsh, P.D., Do, T., Beighton, D. and Devine, D.A. (2016) Influence of saliva on the oral microbiota. *Periodontology 2000*, 70, 80–92.

Mauri-Obradors, E., Estrugo-Devesa, A., Jane-Salas, E., Vinas, M. and Lopez-Lopez, J. (2017) Oral manifestations of diabetes mellitus. A systematic review. *Med Oral Patol Oral Cir Bucal*, 22, e586–e594.

Mellas, R.E., Leigh, N.J., Nelson, J.W., McCall, A.D. and Baker, O.J. (2015) Zonula occludens-1, occludin and E-cadherin expression and organization in salivary glands with Sjögren's syndrome. *Journal of Histochemistry and Cytochemistry*, 63, 45–56.

Nam, K., Maruyama, C.L., Trump, B.G., Buchmann, L., Hunt, J.P., Monroe, M.M. et al. (2016) Post-irradiated human submandibular glands display high collagen deposition, disorganized cell junctions, and

an increased number of adipocytes. *Journal of Histochemistry and Cytochemistry*, 64, 343–352.

Naseri, R., Mozaffari, H.R., Ramezani, M. and Sadeghi, M. (2018) Effect of diabetes mellitus type 2 on salivary glucose, immunoglobulin A, total protein, and amylase levels in adults: a systematic review and meta-analysis of case-control studies. *Journal of Research in Medical Sciences*, 23, 89.

Pathak, K.A., Bhalavat, R.L., Mistry, R.C., Deshpande, M.S., Bhalla, V., Desai, S.B. (2004) Upfront submandibular salivary gland transfer in pharyngeal cancers. *Oral Oncology*, 40, 960–963.

Pedersen, A.M.L., Sorensen, C.E., Proctor, G.B., Carpenter, G.H. and Ekström, J. (2018) Salivary secretion in health and disease. *Journal of Oral Rehabilitation*, 45, 730–746.

Peppi, M. and Ghabriel, M.N. (2004) Tissue-specific expression of the tight junction proteins claudins and occludin in the rat salivary glands. *Journal of Anatomy*, 205, 257–266.

Reuterving, C.O., Hagg, E., Henriksson, R. and Holm, J. (1987) Salivary glands in long-term alloxan-diabetic rats. a quantitative light and electron-microscopic study. *Acta Pathol Microbiol Immunol Scand A*, 95, 131–136.

Salehi, M., Mesgarani, A., Karimipour, S., Pasha, S.Z., Kashi, Z., Abedian, S. *et al.* (2019) Comparison of salivary cortisol level in type 2 diabetic patients and pre-diabetics with healthy people. *Open Access Macedonian Journal of Medical Sciences*, 7, 2321–2327.

Suzuki, A. and Iwata, J. (2018) Molecular regulatory mechanism of exocytosis in the salivary glands. *International Journal of Molecular Sciences*, 19, 3208.

Tiongco, R.E.G., Arceo, E.S., Rivera, N.S., Flake, C.C.D. and Policarpio, A.R. (2019) Estimation of salivary glucose, amylase, calcium, and phosphorus among non-diabetics and diabetics: potential identification of non-invasive diagnostic markers. *Diabetes & Metabolic Syndrome: Clinical Research & Reviews*, 13, 2601–2605.

Xiang, R.L., Mei, M., Cong, X., Li, J., Zhang, Y., Ding, C. *et al.* (2014) Claudin-4 is required for AMPK-modulated paracellular permeability in submandibular gland cells. *Journal of Molecular Cell Biology*, 6, 486–497.

Yang, N.Y., Ding, C., Li, J., Zhang, Y., Xiang, R.-L., Wu, L.-L. *et al.* (2017) Muscarinic acetylcholine receptor-mediated tight junction opening is involved in epiphora in late phase of submandibular gland transplantation. *Journal of Molecular Histology*, 48, 99–111.

Yano, T., Kanoh, H., Tamura, A., Tsukita, S. (2017) Apical cytoskeletons and junctional complexes as a combined system in epithelial cell sheets. *Annals of the New York Academy of Sciences*, 1405, 32–43.

Yoo, D.Y., Yim, H.S., Jung, H.Y., Nam, S.M., Kim, J.W., Choi, J.H. *et al.* (2016) Chronic type 2 diabetes reduces the integrity of the blood-brain barrier by reducing tight junction proteins in the hippocampus. *Journal of Veterinary Medical Science*, 78, 957–962.

Zhang, G.H., Wu, L.L. and Yu, G.Y. (2013) Tight junctions and paracellular fluid and ion transport in salivary glands. *The Chinese Journal of Dental Research*, 16, 13–46.

Zhang, L.W., Cong, X., Zhang, Y., Wei, T., Su, Y.C., Serrão, A. *et al.* (2016) Interleukin-17 impairs salivary tight junction integrity in Sjögren's Syndrome. *Journal of Dental Research*, 95, 784–792.

Zhang, X.M., Huang, Y., Cong, X., Qu, L.-H., Zhang, K., Wu, L.-L. *et al.* (2019) Parasympathectomy increases resting secretion of the submandibular gland in minipigs in the long term. *Journal of Cellular Physiology*, 234, 9515–9524.

Zhang, X.M., Huang, Y., Zhang, K., Qu, L.-H., Cong, X., Su, J.-Z. *et al.* (2018) Expression patterns of tight junction proteins in porcine major salivary glands: a comparison study with human and murine glands. *Journal of Anatomy*, 233, 167–176.

SUPPORTING INFORMATION

Additional supporting information may be found online in the Supporting Information section.

How to cite this article: Huang Y, Mao Q-Y, Shi X-J, et al. Disruption of tight junctions contributes to hyposalivation of salivary glands in a mouse model of type 2 diabetes. *J. Anat.* 2020;00:1–12. https://doi.org/10.1111/joa.13203